PAPER • OPEN ACCESS

Twisting waves increase the visibility of nonlinear behaviour

To cite this article: Grace Richard *et al* 2020 *New J. Phys.* **22** 063021

View the article online for updates and enhancements.

New Journal of Physics

The open access journal at the forefront of physics

PAPER

Twisting waves increase the visibility of nonlinear behaviour

Grace Richard[1], Holly S Lay[1], Daniel Giovannini[1], Sandy Cochran[1], Gabriel C Spalding[2] and Martin P J Lavery[1,3]

[1] School of Engineering, University of Glasgow, Glasgow, United Kingdom
[2] Department of Physics, Illinois Wesleyan, Bloomington, IL 61702, United States of America
[3] Author to whom any correspondence should be addressed.

E-mail: martin.lavery@glasgow.ac.uk

Abstract

Nonlinear behaviour for acoustic systems is readily measured at high acoustic pressures in gasses or bulk materials. However, at low acoustic pressures nonlinear effects are not commonly observed. We find that by phase structuring acoustic beams, one observes evidence of nonlinear behaviour at an acoustic pressure of 66.78 dB lower than non-structured beams in room temperature air. A bespoke 28-element ultrasonic phased array antenna was developed to generate short pulses that carry orbital angular momentum and are propagated over a short air channel. When sampling small areas of the wavefront, we observed a distinctive change in the frequency components near phase singularities. At these phase singularities the local propagation path is screwed, resulting in the collection signals from pulses travelling along different paths across the aperture of a microphone. The usually negligible frequency chirping that arises from nonlinear behaviour in air interfere at these singularity points and produce a distinctive distortion of the acoustic pulse. Simple physical movement in the system or super-sonic wave speeds do not yield similar results. Such distortions in measured frequency response near phase singularities could lead to errors for SONAR or acoustic communication systems, where received signals are integrated over a finite-area detector. With further development this behaviour could potentially lead to accurate measurement techniques for determining a material's nonlinear properties at lower acoustic pressure.

1. Introduction

Harnessing novel properties of shaped wavefronts has become a burgeoning field of study covering optical, radio and acoustic systems. Such systems have enabled optical manipulation [1–3], communications [4–8], sensing [9–12] and quantum information [14–18]. One such form of shaped wavefronts are those that carry orbital angular momentum (OAM), where wavefronts have a distinctive helical phase profile with a centre line discontinuity, known as a singularity [1]. It was first noted that these wavefronts yield an OAM of $\ell\hbar$ per photon by Allen and colleagues in 1992 [19] and are characterised by an azimuthal phase dependence of $\exp(i\ell\theta)$, where θ is the azimuthal coordinate and ℓ can be any integer. In 1999, Hefner and Marston demonstrated the presence of OAM in acoustic waves [20], whose twisted wavefronts result in a local change to the Poynting vector known as the skew angle $\alpha = \frac{\ell}{k \times r}$, where k is the wavenumber and r is the radial position [19], see figure 1. Spatially-patterned wavefronts can be created through the use of controlled ultrasonic transducer arrays and are used extensively for ultrasonic imaging [21]. Recent demonstrations have used controlled arrays to manipulate particles with acoustic tractor beams and to create touch-less haptic interfaces [22–24]. Such systems offer the ability to pattern the wavefront of sound dynamically in a manner similar to the way spatial light modulators do for light, and phased array antennae do for radio waves [25, 26]. Specifically, recent experimental demonstrations have shown that large arrays of

Figure 1. A wavefront that carries OAM will spiral as it propagates through space. (a) Here we show such a wavefront with a topological charge of $\ell = 1$, which specifies both the number of intertwined helices and their pitch. These twisted wavefronts are associated with a change in the local ray direction that varies with radius. (b) Critically, these skewed rays have increased path length as compared to rays representing a planar wavefront. (c) Graphical representation of the local variation in wave-direction that results in a change in phase velocity, v_{p}, determined by the local skew angle α at two particular radii of r_a and r_b, respectively. When recorded by a microphone with a finite aperture, the change in v_{p} will be integrated over the receiver producing a distinctive re-shaping of the recorded pulse with a topological charge of $\ell = 1$.

acoustic transducers can dynamically control an acoustic wavefront, for example, to impart OAM [27–32].

Dispersive media have nonlinear responses to pressure, where the frequency of propagating wave will change with an increase in acoustic pressure and can result in an acoustic pulse being reshaped with a distinctive chirped profile. However, that usually occurs at acoustic pressures close to 194 dB in air [33]. Thus this effect is usually negligible in air with established parameters for nonlinearity around 10 times lower than bulk materials [33, 34]. In acoustics, engineered bulk materials have been demonstrated to change the group velocity of a single acoustic pulse [35, 36]. Similar suggestions of super- or sub-luminal behaviour have been documented in radio in close proximity to a radio antenna, where the speed tends back towards *c* after long-distance propagation [37]. Interference between two independent perpendicularly propagating acoustic signals has been previously considered in bulk materials to enhance nonlinear visibility [38]. In the last few years, some interesting experiments in photonics have demonstrated that a similar effect is possible even in non-dispersive media, such as vacuum, via spatial shaping of a photon's wavefront [39–41]. Experimentally, the time of arrival of a single photon has been shown to change with respect to a comparative photon propagating over a straight optical path, as a result of spatial shaping, potentially indicating a change in the group velocity of the photon [39, 42]. Many of these experiments leave open questions about the interactions between structured wavefronts and dispersive media. One particularly interesting form of structured beams are those that carry OAM with their phase singularities and could reveal unique behaviour in dispersive media.

In this paper, we present experimental results showing that an acoustic pulse with a coherent wavefront that carries OAM increases the visibility of nonlinear behaviour of the propagation sound waves in air, leading to a change in the frequency components of the propagating pulse at acoustic power levels 66.78 dB lower than non-structured beams. A distinctive temporal distortion occurs close to phase singularities, similar to a beat frequency, when structuring a wavefront to carry OAM, figure 2. This beating effect is not observed for a planar wavefront and there is no physical movement in the system. Theoretical analysis confirms this effect will occur when usually negligible nonlinear propagation effects interfere across a wavefront with a spatially varying Poynting vector, which in effect yield local variance in propagation path for structured beams. The effect is most pronounced in areas of rapid change in a wavefront's phase profile, leading to noticeable temporal restructuring and frequency spectrum for a propagation pulse. We present a novel formula that confirms nonlinear behaviour amplification for twisted waves and directly compare this theory to our measured experimental results. This effect can result in perceived Doppler interference that could lead to SONAR systems measuring that a stationary object is moving. Further, with adequate control this effect could also induce errors in time of flight measurements for any receiver with an extended aperture. More broadly, one should consider this effect in radio and optical frequencies at power levels lower than those usually required to observe nonlinear behaviour.
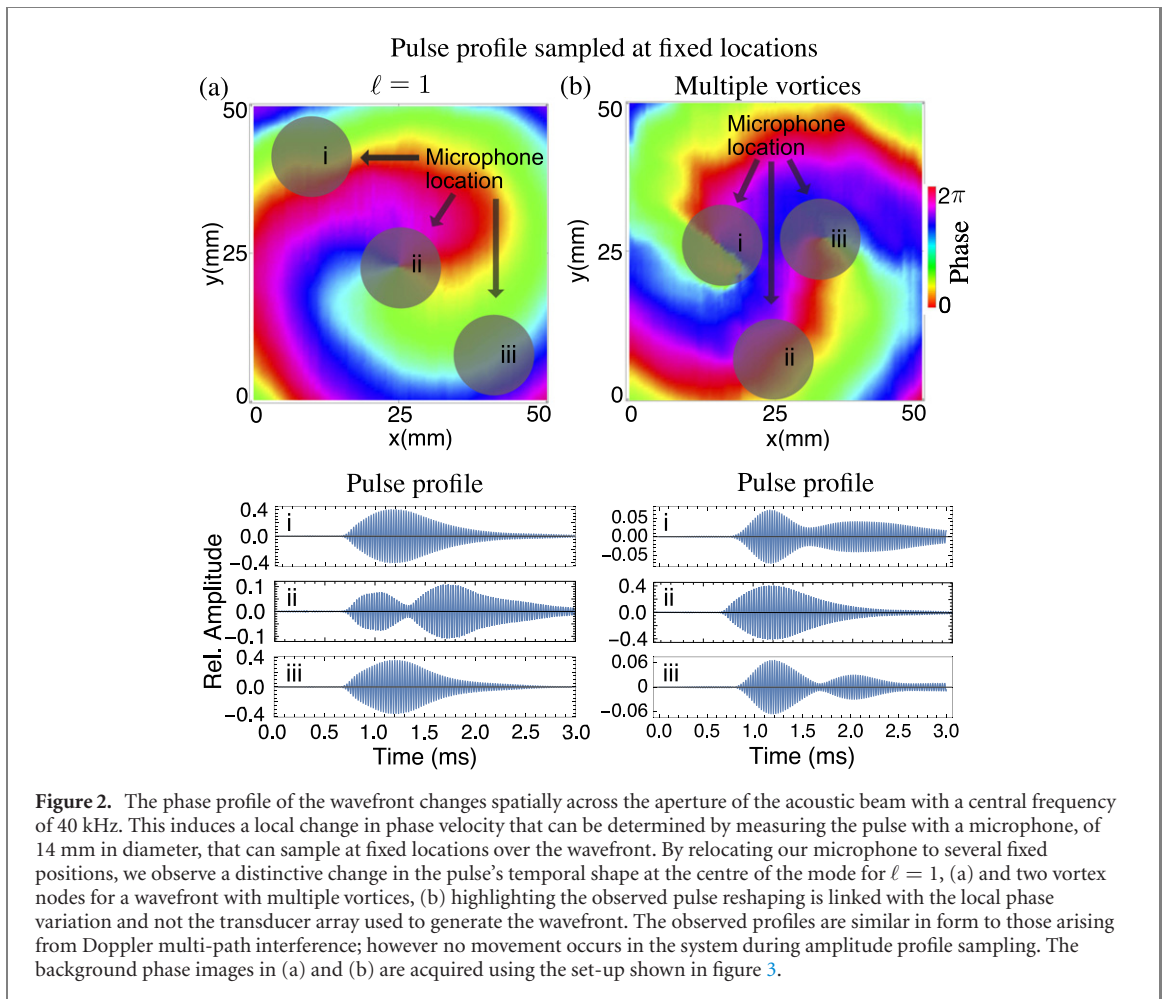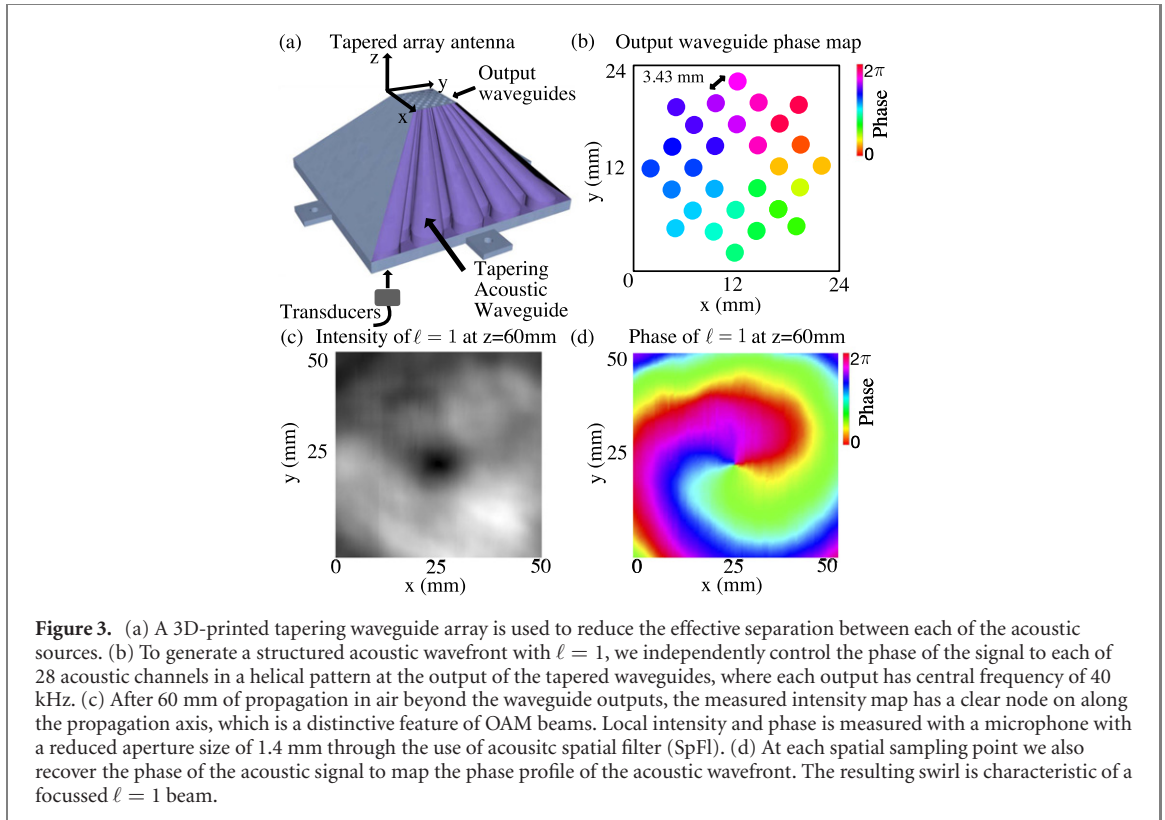
Figure 2. The phase profile of the wavefront changes spatially across the aperture of the acoustic beam with a central frequency of 40 kHz. This induces a local change in phase velocity that can be determined by measuring the pulse with a microphone, of 14 mm in diameter, that can sample at fixed locations over the wavefront. By relocating our microphone to several fixed positions, we observe a distinctive change in the pulse's temporal shape at the centre of the mode for $\ell = 1$, (a) and two vortex nodes for a wavefront with multiple vortices, (b) highlighting the observed pulse reshaping is linked with the local phase variation and not the transducer array used to generate the wavefront. The observed profiles are similar in form to those arising from Doppler multi-path interference; however no movement occurs in the system during amplitude profile sampling. The background phase images in (a) and (b) are acquired using the set-up shown in figure 3.

2. Experimental design

We experimentally generated our structured wavefront with a bespoke array antenna with 28 independently controlled air-coupled ultrasonic transducers with a resonant frequency of 40 kHz with a bandwidth of 1 kHz (MCUSD14A40S09RS-30C, Premier Farnell, Leeds, UK). Each transducer was driven by a 0–5 V square-wave digital signal with a frequency of 40 kHz generated by a digital input/output device (USB-6255, National Instruments, Austin, TX, USA). The resonance of the transducer material leads to the generation of air coupled sine waves. The phase of the driving square wave can be individually tuned for each transducer. This tuning allows direct control of the local acoustic phase.

The distance between adjacent acoustic sources is very important to generate a coherent acoustic wavefront as one can readily generate grating lobes that would represent significant artefacts in the generation of our desired wavefront. As our transducers have a physical aperture size of 14 mm, we developed an integrated custom array of acoustic waveguides, manufactured through additive manufacturing and made from PLA (polylactic acid), to allow for close packing of the 28 acoustic sources, shown in figure 3(a). Each circular waveguide had an output diameter of 2.4 mm arranged in a square grid with a pitch of 3.43 mm. This spacing is half the acoustic wavelength, which in optics would mean that our waveguides would not guide light due to being sub-wavelength in diameter, however for longitudinal sound waves this limit does not exist and ensures we generate a spatially coherent wavefront. Such tapered waveguides suppress potential grating lobes by pushing the first-order minima beyond 180°, this suppression leads to acoustic absorption of 7 dB. For the given drive signals, the peak sound pressure from each transducer is approximately 90 dB at standard measurement distance of 1 m, leading to a total sound pressure for all 28 elements of 92 dB, including waveguide loses. We note acoustic power will vary with distance from the array.

As phase-only modulation was used to generate our structured wavefronts, we required accurate calibration to phase match the waveguide outputs from the 28 independent transducers. Two sources of systematic phase error in our array antenna are the differences in path lengths of each of the acoustic

Figure 3. (a) A 3D-printed tapering waveguide array is used to reduce the effective separation between each of the acoustic sources. (b) To generate a structured acoustic wavefront with $\ell = 1$, we independently control the phase of the signal to each of 28 acoustic channels in a helical pattern at the output of the tapered waveguides, where each output has central frequency of 40 kHz. (c) After 60 mm of propagation in air beyond the waveguide outputs, the measured intensity map has a clear node on along the propagation axis, which is a distinctive feature of OAM beams. Local intensity and phase is measured with a microphone with a reduced aperture size of 1.4 mm through the use of acousitc spatial filter (SpFl). (d) At each spatial sampling point we also recover the phase of the acoustic signal to map the phase profile of the acoustic wavefront. The resulting swirl is characteristic of a focussed $\ell = 1$ beam.

waveguides and electrical impedance differences between each of the transducers. To overcome the path-length difference, a specific time delay was added to each of the transducers based on precise measurement of the length of each waveguide, which vary between 44 mm and 58 mm in length. To overcome impedance induced phase errors that resulted in sub-wavelength differences between each transducer, we directly measured the acoustic wave generated at each of the array output ports. The relative phase difference between each transducer was determined by computational comparison with a reference sine wave, matching the air-coupled waves generated by the transducers. By adding the measured phase offset to each of the transducers, the array was fully calibrated to provide a flat acoustic wavefront.

To generate a specific acoustic wavefront, the phase term, ϕ, for each transducer is set based on azimuthal position, θ, such that $\phi = \exp(i\ell\theta)$, shown in figure 3(b). Initially using a microphone with a 25–530 kHz operational input frequency range (R3a 1232-1, Mistras, New Jersey, USA), the signal bandwidth for a range of ℓ values was determined to be within the range 38–42 kHz. Subsequently, a high efficiency microphone with a suitable measurement sensitivity (MCUSD14A40S09RS-30C, Premier Farnell, Leeds, UK) was used record the presented data. Using this microphone we measured the intensity and relative phase over a 50×50 mm^2 region by scanning it with a spatial resolution of 0.5 mm (figures 3(c) and (d)). The microphone has a circular active area with a diameter of 14 mm that was reduced to a diameter 1.2 mm through the use of a discriminating cone made of PLA.

3. Results and discussion

The propagation speed of a pulse can generally be separated into the speed of propagation of the pulse's amplitude envelope, i.e., the group velocity, v_g, and the propagation speed of the phase, i.e., the phase velocity v_p [43]. The phase velocity along the beam axis is determined by the angular frequency, ω, and the axial component of the local wave vector, k_z, as

$$v_p = \frac{\omega}{k_z}. \tag{1}$$

In the case of a mode with a plane wavefront propagating along the optic axis, k_z is precisely defined as $k_z = k_0 = 2\pi/\lambda$. However, for structured modes there is a local variation in $\vec{k}$ arising from the phase change across its wavefront [19]. For beams that carry OAM the wavefront is locally skewed, leading to a variation in $\vec{k}$ that is dependent on ℓ and r, as shown in figure 1(c).

To investigate the spatial variance of nonlinear behaviour that will locally effect v_p across the patterned acoustic wavefront, we generated a single Gaussian shaped pulse with the profile, $P \exp\left(\frac{(t - \mathrm{d}t)^2}{\sigma^2}\right)$, where the

standard deviation is approximately $\sigma = 0.5$ ms and peak power P. We can mathematically represent this pulse by a travelling sine wave with time, t, varying amplitude, $A(t)$, as

$$\psi = A(t) \sin (k_0 x - \omega t + \Phi).$$ (2)

where ω is the angular frequency ($\omega = 2\pi f$). The majority of gases and material have a non-linear response that varies with acoustic pressure. This results in the propagating wave leading to local heating as the waves are transferred through that material and alters the propagation speed of sound. This change in velocity is given by [33]

$$c = c_0 + \frac{1}{2\rho_0 c_0} \left(\frac{B}{A} \right) \Delta P$$ (3)

where $\frac{B}{A}$ is the nonlinear parameter, P is the dynamic acoustic pressure, ρ is the density of air, c_0 is the speed of sound. For a propagation wave this non-linear parameter results in a phase shift, $\Delta \phi$ along a given path, Δx, that is given by [38]

$$\Delta \phi = -\omega \frac{1}{2\rho_0 c_0^3} \left(\frac{B}{A} \right) \Delta P \Delta x.$$ (4)

The local skewing of rays spatially alters the path the wavefront is travelling, therefore for acoustic wavefronts carrying OAM the path term must be modified to be

$$\Delta x = \frac{c_0 \Delta t}{\cos \left(\frac{\ell}{kr} \right)}.$$ (5)

Within our experimental system, we have a finite area detector that has a circular aperture that samples a portion of the wavefront between radial positions r_a and r_b. The detector measures the superposition of multiple locally skewed rays that vary as α. Therefore, by replacing the path dependent phase term represented equation (4) into the standard form of a propagation sine wave, shown in equation (2), we can express the expected amplitude profile for twisted acoustic wavefronts as
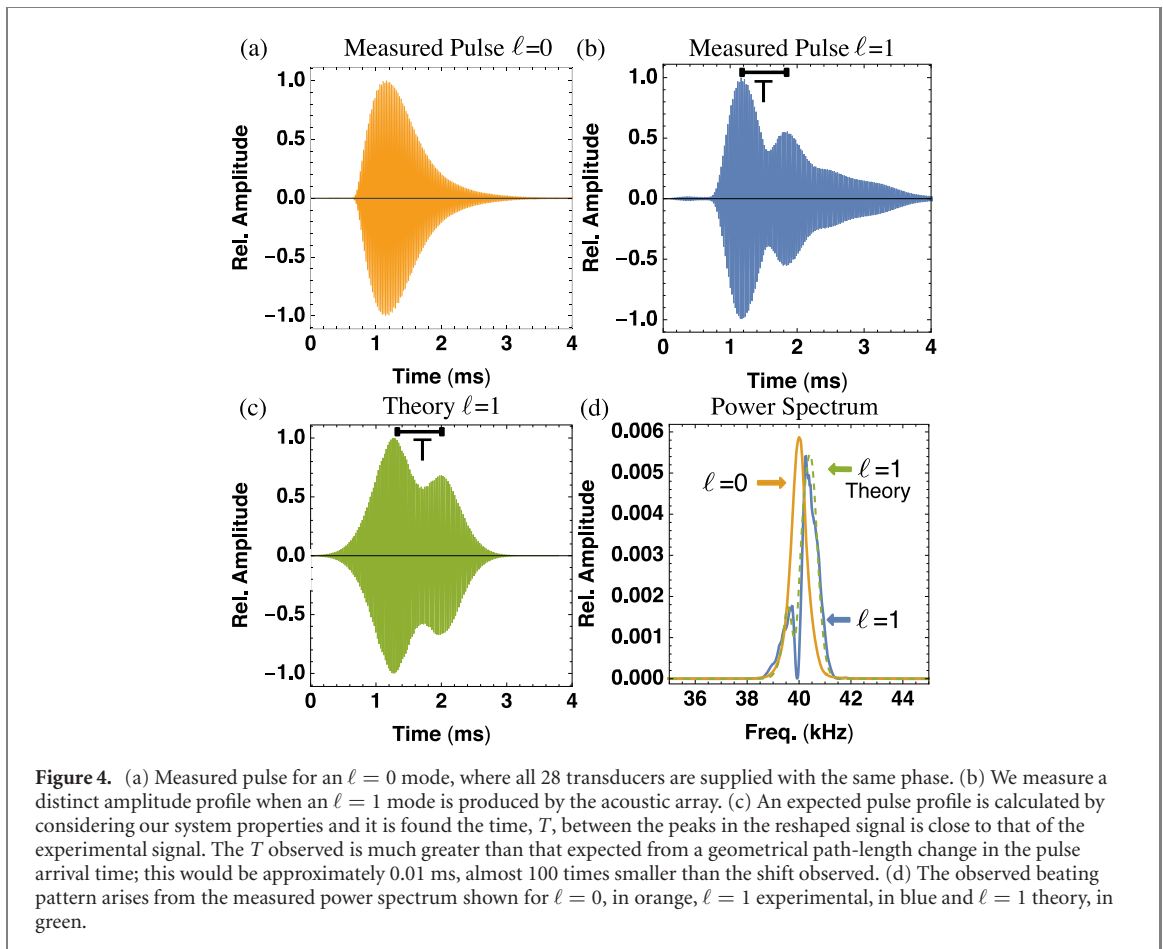
$$\psi = \int_{r_a}^{r_b} \int_{-\pi}^{+\pi} P \exp \left(\frac{-(t - \mathrm{d}t)^2}{\sigma^2} \right) \cos \left(k_z z - 2\pi f_0 t - \left(\frac{c_o t}{\cos \left(\frac{\ell}{kr} \right)} \right) \left(\frac{f_0 \frac{B}{A}}{2\rho c_0^3} \right) P \exp \left(\frac{-(t - \mathrm{d}t)^2}{\sigma^2} \right) \right) r \mathrm{d}\theta \mathrm{d}r,$$ (6)

where t is time, $\mathrm{d}t$ is the time delay from pulse propagation time to the microphone, ΔP is the dynamic acoustic pressure equal to 7.83 dB per mm^2 at a propagation distance of $z = 60$ mm from the output, ρ is the density of air, c_0 is the speed of sound in air at 20° Celsius and established non-linear parameter for air of $\frac{B}{A} = 0.4$ [34]. The total power over the aperture of the microphone is 127.22 dB. By considering the equation (6), and the physical aperture size and position of our microphone, we computed an expected amplitude profile and frequency response, figures 4(c) and (d) respectively.

The spatially varying path results in superposition of the propagating waves, any small chirping arising from non-linear behaviour will in turn reshape the amplitude profile, ψ. As with all superpositions, the particular shaper of a pulse will be determined by the particular position along its path of propagation, z, as the temporal profile of the pulse observed is an integral of the local change in phase velocity over a given receiver.

We can readily make an experimental acoustic measurement to confirm the pulse amplitude profile, as seen in figures 2 and 4, which match the profiles computed from equation (3). For a flat wavefront, $\ell = 0$, sampled at the centre of the acoustic mode, we measured an elongated pulse with a centre frequency of $f_0 = 40$ kHz, figures 4(a) and (d). This pulse elongation arises from the impulse response of the transducers, which are designed to have a 40 kHz resonant characteristic.
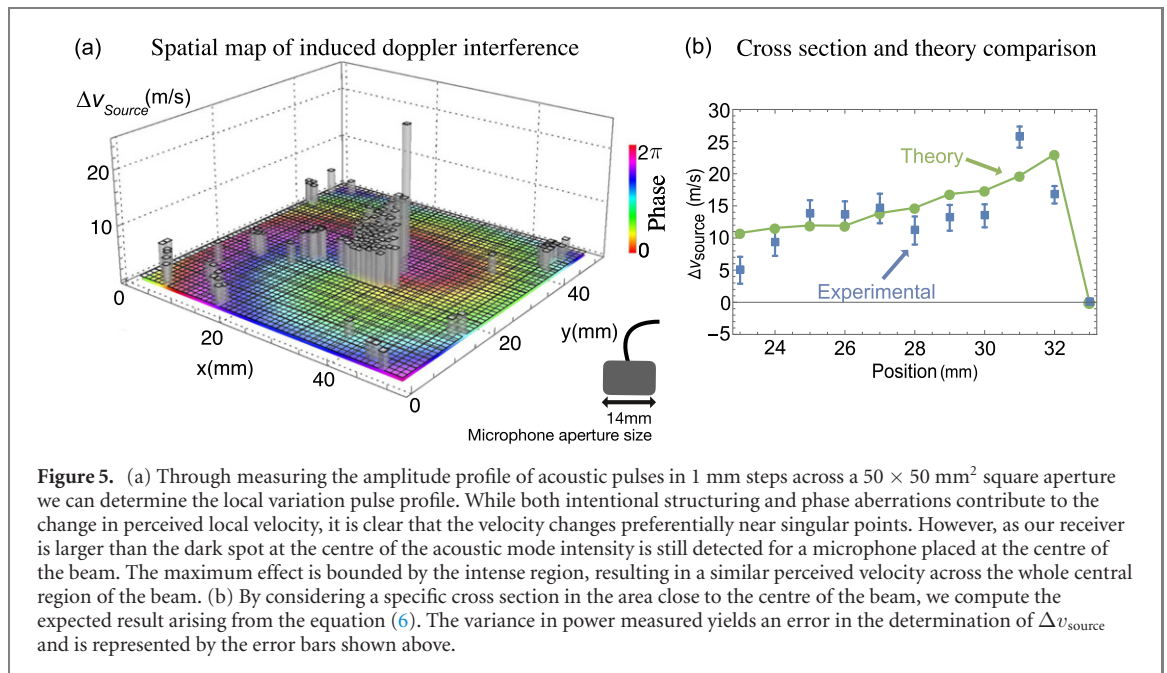
Adapting nothing apart from the spatial wavefront profile, to carry $\ell = 1$, we measured a pulse profile indicating significant reshaping when our microphone is placed at the centre of the twisted acoustic mode, figure 4(b). This change in amplitude indicates a change in the interference between composite frequency components comprising the pulse itself, and the superposition of wavefronts that combine at the microphone. In the frequency domain, it can be seen in figure 4(d) that the centre frequency of the reshaped pulse is at the carrier frequency 40 kHz with profile corresponding to a set of extra frequency components confirming a phase velocity change and not a temporal delay in arrival time. We expect the slight difference in measured frequency components for $\ell = 1$ as seen in figure 4(d) is from the spectral efficiency of our microphone and harmonics from background noise. It should be noted similar pulse reshaping has been observed with the 25–530 kHz microphone, however with higher level of electrical noise due to lower microphone sensitivity. The theoretical acoustic frequency spectrum is filtered to match the frequency response of the experimental microphone. We further measured that the detected pulse

Figure 4. (a) Measured pulse for an $\ell = 0$ mode, where all 28 transducers are supplied with the same phase. (b) We measure a distinct amplitude profile when an $\ell = 1$ mode is produced by the acoustic array. (c) An expected pulse profile is calculated by considering our system properties and it is found the time, T, between the peaks in the reshaped signal is close to that of the experimental signal. The T observed is much greater than that expected from a geometrical path-length change in the pulse arrival time; this would be approximately 0.01 ms, almost 100 times smaller than the shift observed. (d) The observed beating pattern arises from the measured power spectrum shown for $\ell = 0$, in orange, $\ell = 1$ experimental, in blue and $\ell = 1$ theory, in green.

re-shaping (beating pattern) visibility is higher with an increase in the diameter of the detector aperture, further reinforcing the role integrating over an extended aperture plays in this observation.

From equation (2), the phase velocity will change with radius, r. Hence, we repositioned our microphone to record the full pulse profile at several fixed locations. It can be seen in figure 2(a) that the pulse amplitude appears similar to the $\ell = 0$ case at larger radii. This is consistent with a smaller change in phase velocity at these positions in the wavefront. To confirm our observations are induced by the patterned wavefront, we generated a more complex wavefront comprising two spatially separated acoustic vortices, figure 2(b). Our system has relatively low spatial resolution with only 28 transducers and is mildly phase aberrated, therefore we can readily achieve spatially separated vortices by simply programing our phase array antenna to have an azimuthal phase variation of $\exp(i2\theta)$ [6, 44]. This vortex splitting further confirms the coherent nature of the acoustic wavefront [44]. Moving the position of the microphone to measure the pulse profile at the centre of each vortex shows a pulse reshaping similar to $\ell = 1$, figure 2(b). Hence, these results show that this pulse reshaping arises from spatial phase profile and not simply an artefact from a particular impedance response for a select few transducers placed near the middle of our array.

Doppler sonar is one widely used technique that could be confused by increase visibility of nonlinear behaviour, where beats on received signals indicate movement of a target [45]. These techniques determine time delays between peaks in the pulse amplitude profile to predict a perceived detector of a moving object but considering the beat arising from the Doppler effect. Two waves with slightly different frequencies will beat to an amplitude variation with $1/T = f_{r_a} - f_{r_b}$. This principle is central to the field of Doppler velocimetry, where the measurement of this beat is used to determine the speed of a moving object [45]. Hence, through determination of the time between the pulse amplitude peaks, we calculate the perceived change in measured speed at any particular location in the acoustic wavefront that carries OAM. To calculate the local speed change, we determine T at 1 mm steps across the entire 50×50 mm^2 sampling aperture, figure 5. In certain cases only one peak is detected. However, the effective T can be calculated through fitting of the theoretically expected peak position movement with respect to a pulse generated with a planar wavefront. By computing the expected source velocity from the induced Doppler like interference, we expect to see an increase in Δv_{source} at the centre of the acoustic vortex. The dark area, arising from destructive interference, located at the centre of phase vortices, will limit the maximum observable phase

Figure 5. (a) Through measuring the amplitude profile of acoustic pulses in 1 mm steps across a 50×50 mm^2 square aperture we can determine the local variation pulse profile. While both intentional structuring and phase aberrations contribute to the change in perceived local velocity, it is clear that the velocity changes preferentially near singular points. However, as our receiver is larger than the dark spot at the centre of the acoustic mode intensity is still detected for a microphone placed at the centre of the beam. The maximum effect is bounded by the intense region, resulting in a similar perceived velocity across the whole central region of the beam. (b) By considering a specific cross section in the area close to the centre of the beam, we compute the expected result arising from the equation (6). The variance in power measured yields an error in the determination of Δv_{source} and is represented by the error bars shown above.

velocity due to the limited dynamic range of the microphone and amplifier used for our experimental measurements. Nevertheless, our results show a clear change in v_{p} close to the vortex core for $\ell = 1$, see figure 5. We do also observe several locations at higher radius with pulse deformations, which we suspect arises from local phase aberrations in the wavefront. Further detailed studies into the contribution of aberrations to the shape of measured pulses will be conducted in future work. That is, smaller wavefront aberrations can result in local changes in phase velocity due to the locally skewed rays, which we observed in the peaks located away from the centre of figure 5. More significantly, near the singular point we observe a peak $\Delta v_{\text{source}} = 25.0$ ms^{-1} and average $\Delta v_{\text{source}} = 1.1$ ms^{-1} for $\ell = 1$. Consistent behaviour is observed in the results obtained with multiple singular points.

4. Conclusions

Airborne acoustic fields have afforded us the ability to fully explore the details of structured wavefront propagation in a way that is more difficult in optics. Our experimental results indicate a change in phase profile will yield reshaping of a propagating pulse, as shown in figures 2(a) and (b). This pulse reshaping arises that from the increased visibility of non-linear behaviour will result in beat patterns that appear as a change in the pulse peak position and could result in the potential impression of altered arrival time. Hence, controlled spatial variation in phase or spatial phase aberrations could be used to induce measurement errors in the arrival time of a particular pulse by inducing Doppler like interference when there is no physical movement by the sender or receiver. We demonstrated this effect can lead to a perceived change in source velocity of $\Delta v_{\text{source}} > 10$ ms^{-1}. This induced Doppler inference could be critically important for SONAR, RADAR and LIDAR, especially where only a subsection of the entire wavefront is collected by a detector. Further, the pulse amplitude variation could result in errors for experimental systems that lock to a reference signal, such as heterodyne detectors or Hong–Ou–Mandel interference when light is collected over areas of local variance in phase velocity as usually negligible non-linear effects can be amplified for an extended receiver. Further, the beating observed could be a fundamentally limiting factor in the effective deployment of spatial multiplexing in acoustic communications. Producing a propagating acoustic field such that a vortex is positioned at the aperture of Doppler-sonar or an acoustic communication system could be used to manipulate the performance of these systems.

Acknowledgments

ORCID iDs

Martin P J Lavery ⬤ https://orcid.org/0000-0001-6419-421X

References

[1] Allen L, Barnett S M and Padgett M J 2003 *Optical Angular Momentum* (Bristol: Institute of Physics Publishing)
[2] Andrews D L 2008 *Structured Light and its Applications: An Introduction to Phase-Structured Beams and Nanoscale Optical Forces* (Amsterdam: Academic)
[3] Rubinsztein-Dunlop H *et al* 2017 *J. Opt.* **19** 13001
[4] Gibson G *et al* 2004 *Opt. Express* **12** 5448
[5] Lavery M P J *et al* 2017 *Sci. Adv.* **3**
[6] Lavery M P J 2018 *New J. Phys.* **20** 043023
[7] Huang H *et al* 2015 *Sci. Rep.* **5**
[8] Rusch L A, Rad M, Allahverdyan K, Fazal I and Bernier E 2018 *IEEE Commun. Mag.* **56** 219
[9] Lavery M P J, Speirits F C, Barnett S M and Padgett M J 2013 *Science* **341** 537
[10] Arita Y, Mazilu M and Dholakia K 2013 *Nat. Commun.* **4**
[11] Ritsch-Marte M 2017 *Phil. Trans. R. Soc.* A **375**
[12] Monteiro F, Ghosh S, van Assendelft E C and Moore D C 2018 *Phys. Rev.* A **97** 051802
[13] Hau L V, Harris S E, Dutton Z and Behroozi C H 1999 *Nature* **397** 594
[14] Leach J, Padgett M J, Barnett S M, Franke-Arnold S and Courtial J 2002 *Phys. Rev. Lett.* **88** 257901
[15] Franke-Arnold S *et al* 2004 *New J. Phys.* **6**
[16] Malik M *et al* 2014 *Nat. Commun.* **5**
[17] Fickler R, Campbell G, Buchler B, Lam P K and Zeilinger A 2016 *Proc. Natl Acad. Sci.* **113** 13642
[18] Wang X-L *et al* 2018 *Phys. Rev. Lett.* **120** 260502
[19] Allen L, Beijersbergen M W, Spreeuw R J C and Woerdman J P 1992 *Phys. Rev.* A **45** 8185
[20] Hefner B T and Marston P L 1999 *J. Acoust. Soc. Am.* **106** 3313
[21] Smith S 1992 *Ultrason. Imaging* **14** 213
[22] Démoré C E M *et al* 2014 *Phys. Rev. Lett.* **112** 174302
[23] Long B, Seah S A, Carter T and Subramanian S 2014 *ACM Trans. Graph.* **33**
[24] Seah S A, Drinkwater B W, Carter T, Malkin R and Subramanian S 2014 *IEEE Trans. Ultrason. Ferroelectr. Freq. Control* **61** 1233
[25] Konforti N, Marom E and Wu S T 1988 *Opt. Lett.* **13** 251–3
[26] Cochran S 2006 *Insight* **48** 212
[27] Volke-Sepulveda K, Santillan A O and Boullosa R R 2008 *Phys. Rev. Lett.* **100** 024302
[28] Skeldon K D, Wilson C, Edgar M and Padgett M J 2008 *New J. Phys.* **10**
[29] Demore C E M *et al* 2012 *Phys. Rev. Lett.* **108** 194301
[30] Anhauser A, Wunenburger R and Brasselet E 2012 *Phys. Rev. Lett.* **109** 034301
[31] Marzo A, Caleap M and Drinkwater B W 2018 *Phys. Rev. Lett.* **120** 044301
[32] Gibson G M *et al* 2018 *Proc. Natl Acad. Sci.* **115** 3800
[33] Beyer R T and Letcher S V 1969 *Physical Ultraonsics* (New York: Academic)
[34] Hamilton M F and Blackstock D T 2008 *Nonlinear Acoustics* (Acoustical Society of America)
[35] Zhu X *et al* 2016 *Nat. Commun.* **7** 11731
[36] Lemoult F, Kaina N, Fink M and Lerosey G 2013 *Nat. Phys.* **9** 55–60
[37] Mugnai D, Ranfagni A and Ruggeri R 2000 *Phys. Rev. Lett.* **84** 4830
[38] Ichida N, Sato T, Miwa H and Murakami K 1984 *IEEE Trans. Sonics Ultrason.* **31** 6
[39] Giovannini D *et al* 2015 *Science* **347** aaa3035
[40] Bouchard F, Harris J, Mand H, Boyd R W and Karimi E 2016 *Optica* **3** 351
[41] Lyons A *et al* 2018 *Optica* **5** 682
[42] Bareza N D and Hermosa N 2016 *Sci. Rep.* **6** 857
[43] Brillouin L 1960 *Wave Propagation and Group Velocity* (New York: Academic)
[44] Basistiy I V, Bazhenov V Y, Soskin M S and Vasnetsov M V 1993 Optics of light beams with screw dislocations *Opt. Commun.* **103** 422–8
[45] Durst F *et al* 1976 *Principles and Practice of Laser Doppler Anemometry* (New York: Academic)